JGR Atmospheres

RESEARCH ARTICLE
10.1029/2018JD030207

Arctic Summer Sea Ice Melt and Related Atmospheric Conditions in Coupled Regional Climate Model Simulations and Observations

A. Rinke[1], Erlend M. Knudsen[2], D. Mewes[3], W. Dorn[1], D. Handorf[1], K. Dethloff[1], and J. C. Moore[4,5,6]

[1]Alfred Wegener Institute, Helmholtz Centre for Polar and Marine Research, Potsdam, Germany, [2]Institute for Geophysics and Meteorology, University of Cologne, Cologne, Germany, [3]Institute for Meteorology, University of Leipzig, Leipzig, Germany, [4]College of Global Change and Earth System Science, Beijing Normal University, Beijing, China, [5]Arctic Centre, University of Lapland, Rovaniemi, Finland, [6]CAS Center for Excellence in Tibetan Plateau Earth Sciences, Beijing, China

Abstract Observations from 1979 to 2014 show a positive trend in the summer sea ice melt rate with an acceleration particularly in June and August. This is associated with atmospheric circulation changes such as a tendency toward a dipole pattern in the mean sea level pressure (SLP) trend with an increase over the Arctic Ocean and a decrease over Siberia. Consistent with previous studies, we here show the statistical relationship between the summer sea ice melt rate and SLP and that more than one SLP pattern is associated with anomalously high melt rates. Most high melt rates occur during high pressure over the Arctic Ocean accompanied by low pressure over Siberia, but a strong Beaufort High and advection of warm air associated with a cyclone located over the Taymyr Peninsula can also trigger anomalous high ice melt. We evaluate 10-member ensemble simulations with the coupled atmosphere-ice-ocean Arctic regional climate model HIRHAM-NAOSIM. The simulations have systematically low acceleration of sea ice melt rate in August, related to shortcomings in representing the strengthening pressure gradient from the Barents/Kara Sea toward Northern Greenland in recent decades. In general, the model shows the same classification of SLP patterns related to anomalous melt rates as the observations. However, the evolution of sea ice melt-related cloud-radiation feedback over the summer reveals contrary effects from low-level clouds in the reanalysis and in the simulations.

Key Points:
- Trends in Arctic sea ice melt rate and mean sea level pressure in summer months May–August 1979–2014 are quantified
- Coupled regional climate simulations reproduce observed statistical relation between melt rate and atmospheric circulation, but show deficits in August
- Contrary sea ice melt-related cloud-radiation feedback evolving over the summer are found

Supporting Information:
- Supporting Information S1

Correspondence to:
A. Rinke,
Annette.Rinke@awi.de

Citation:
Rinke, A., Knudsen, E. M., Mewes, D., Dorn, W., Handorf, D., Dethloff, K., & Moore, J. C. (2019). Arctic summer sea ice melt and related atmospheric conditions in coupled regional climate model simulations and observations. *Journal of Geophysical Research: Atmospheres*, *124*, 6027–6039. https://doi.org/10.1029/2018JD030207

Received 21 DEC 2018
Accepted 18 MAY 2019
Published online 18 JUN 2019
Corrected 29 JUL 2019

This article was corrected on 29 JUL 2019. See the end of the full text for details.

1. Introduction

One of the apparent features of the rapid Arctic climate change, the so-called Arctic amplification (Serreze & Barry, 2011; Wendisch et al., 2017), is the observed Arctic sea ice loss in summer and its implications for the climate and the ecosystem (Meier et al., 2014). Climate models still show limitations in simulating a realistic sea ice loss (e.g., Dorn et al., 2012; Stroeve et al., 2012), which indicates that many coupled climate system processes are not well understood or not adequately represented in the models. Generally, atmospheric circulation and related processes strongly control the summer sea ice extent and its variability from year to year. This includes the impact on sea ice drift by near-surface winds and the impact on sea ice melt by atmospheric conditions such as clouds and radiation (Döscher et al., 2014). Sea ice loss in summer is influenced by both cyclones and anticyclonic circulation anomalies. The impact of cyclones is important but complex (Wernli & Papritz, 2018). While in general fewer cyclones throughout the summer favor a stronger sea ice loss (Knudsen et al., 2015; Screen et al., 2011), the occurrence of intense cyclones can cause a strong ice loss, particularly in late summer (Simmonds & Rudeva, 2012; Zhang et al., 2013).

Many studies have shown that summer sea ice anomalies are statistically correlated with summer atmospheric circulation patterns (e.g., Knudsen et al., 2015; Lynch et al., 2016; Mills & Walsh, 2014; Serreze et al., 2016; Zhang et al., 2018). Ding et al. (2017) attributed 60% of the late summer sea ice retreat to the trend in the summer mean atmospheric circulation. Generally, years characterized by anomalously low (high) Arctic sea ice extent are typically associated with the presence of a strong (weak) Beaufort High and anticyclonic (cyclonic) circulation over the Arctic Ocean. However, such a view is oversimplified because of the large variability of the summer atmospheric circulation both from year to year and from month to month, resulting in combinations of circulation patterns that can induce similar sea ice extent

anomalies in summer (Serreze et al., 2016). We find it instructive, therefore, to examine sea ice retreat during individual summer months in combination with the complete range of synoptic patterns. This synoptic variability of the atmospheric circulation connected to enhanced baroclinicity becomes increasingly important under the ongoing sea ice reduction and thinning and an associated higher ice mobility. An improved understanding of the linkages between sea ice anomalies and atmospheric circulation can help improve the overall and spatial prediction of the sea ice retreat in the summer months (e.g., Guemas et al., 2016; Stroeve et al., 2015), which is important for industrial activities (e.g., shipping, resource extraction) and local communities.

In contrast to other studies, we analyze sea ice melt rather than sea ice extent, because the former is a more direct measure of sea ice changes resulting from, and leading to, alteration in atmospheric patterns (Knudsen et al., 2015). Our analysis focuses on the Arctic north of approximately 60°N and over the extended summer, May–August, for the 1979–2014 period. We discuss the observed monthly summer sea ice melt rates and atmospheric circulation (represented by mean sea level pressure (SLP)) and their trends, as well as relations between both variables. In addition to a correlation and composite analysis considering anomalously low and high sea ice melt conditions, we apply the self-organizing map (SOM) technique. SOM makes use of an artificial neural network (Kohonen, 1998) to determine a set of representative weather patterns. Liu et al. (2006) showed that SOM analysis has an advantage compared to other pattern detection methods, since it is able to extract nonlinear and asymmetric features. This method has been shown to be a useful tool for studying atmospheric circulation changes in connection with sea ice cover changes (Higgins & Cassano, 2009; Lynch et al., 2016; Mills & Walsh, 2014).

For coupled climate models to be successful in sea ice simulations, it is important that they capture the linkages between atmospheric circulation and sea ice, and related feedback. Therefore, it is important to describe, and compare, how the sea ice anomalies in climate models are related with atmospheric circulation patterns. Accordingly, another aim of our study is to examine how well ensembles of state-of-the-art coupled Arctic regional climate model simulations capture the observed trends of sea ice melt rate and SLP, and the sea ice-atmospheric circulation relationship in summer.

2. Data and Analysis

2.1. Model Simulations and Observational Data

We analyze 10-member ensemble simulations from the coupled atmosphere-ice-ocean Arctic regional climate model HIRHAM-NAOSIM (Dorn et al., 2009), which includes improved Arctic regional process descriptions that can reproduce observed atmosphere-sea ice relationships (Dorn et al., 2012; Rinke et al., 2013). The model simulations were laterally driven by the European Centre for Medium-Range Weather Forecasts Interim reanalysis (ERA-Interim; Dee et al., 2011) and cover the 36-year period from 1979 to 2014. All 10 ensemble members were started equally on 1 January 1979 and run through 31 December 2014. The runs only differ by their initial ice-ocean fields, which were taken from different years of a preceding run (Dorn et al., 2012). For details on the simulation setup, we refer to Graham et al. (2017) and Rinke et al. (2018).

The main observational data sets we used for comparison to the model are (i) SLP, downward longwave (LWD) and shortwave radiation at the surface (SWD), and total cloud cover from ERA-Interim and (ii) sea ice concentration (SIC) data from the National Snow and Sea Ice Data Center (Cavalieri et al., 1996). This SIC product provides a consistent SIC time series spanning the coverage of several passive microwave instruments and has been generated using the NASA Team algorithm (https://nsidc.org/data/NSIDC-0051/). The SIC data were bilinearly interpolated onto the model grid before sea ice extent (SIE) was calculated. ERA-Interim data were also remapped onto the model grid using bilinear interpolation to compare with the simulations.

2.2. Analysis Methods

We follow Knudsen et al. (2015) in the calculation of composites for low and high sea ice melt years, based on the sea ice melt rate anomaly. The monthly sea ice melt rate was defined as the difference between the SIE from the first and the last day of the month. From this, standardized sea ice melt rates were calculated for each summer month by subtracting the long-term averaged monthly melt rate from

the actual monthly melt rate and then dividing by the standard deviation of the monthly melt rate. The threshold of ±1 of the standardized melt rates defined months of anomalously high melt rate (HMR) and of anomalously low melt rate (LMR). For the observations, the HMR and LMR composites come from 25 and 17 months, while for the HIRHAM-NAOSIM ensemble simulation, the HMR and LMR composites are based on 252 and 242 months, respectively (Figure S1 in the supporting information). Although the composites from the observations and the model include different years and thus different regional sea ice anomalies and synoptic circulations, our results are robust: using only common months to make the composites does not change our findings. Using the full composite set of months provides better statistics. Composites of atmospheric parameters (SLP, LWD, SWD, total cloud cover) were calculated for the selected HMR and LMR cases. The difference "HMR minus LMR" serves as a measure for differences in atmospheric conditions under anomalous sea ice melt. Their statistical significance has been calculated with the Student's t test.

We compliment the composite analysis with two other methods to further analyze the atmospheric circulation associated with sea ice melt anomalies: (i) correlations between detrended time series of sea ice melt rate and SLP in summer and (ii) SOM analysis of monthly SLP patterns. SOM is an artificial neural network method, used to reduce the dimensionality of data based on the python package "somoclu" (Wittek et al., 2017). The SLP fields of all 36 years of each of the 10 individual HIRHAM-NAOSIM simulations and the ERA-Interim data were subjected to SOM analysis. Locations with surface elevations higher than 500 m were removed from the SLP fields because pressure reduction to sea level can lead to unrealistic singularities emerging in the SOM, which may then obscure realistic patterns (Higgins & Cassano, 2009). After inspecting several SOM array dimensions (4 × 3, 5 × 4, 7 × 5), we selected a size of 5 × 4. This grid is large enough to capture the major circulation patterns and small enough to assign important differences among the patterns, a conclusion similar to that reached by Lynch et al. (2016). The HMR and LMR cases were grouped according to the calculated SOM.

Linear trends of sea ice melt rate and SLP were calculated by linear least squares regression, with statistical significance assessed by a bootstrapping method. We used the pattern correlation coefficient to quantify similarity in the observed and simulated spatial patterns.

3. Results

First, we describe and compare the climatology, interannual variability, and trend of both the sea ice melt rate (section 3.1) and the SLP field (section 3.2). Afterward, we analyze the atmospheric circulation associated with anomalous sea ice melt rates (section 3.3).

3.1. Sea Ice Melt Rate

Observed sea ice melt rates show a distinct monthly cycle within the summer season (Figure 1). While the lowest melt rate (0.5 Mill. km^2) typically occurs at the beginning of the summer in May, the highest melt rate occurs in midsummer in July with a mean rate of 1.9 Mill. km^2 (Table 1). The time series of the melt rates exhibit considerable interannual variability, with the highest amplitude (maximum minus minimum melt rate within the 36 years) of 1.5 Mill. km^2 in August and the lowest of 0.5 Mill. km^2 in May. Superimposed on the year-to-year variability, significant positive melt rate trends over 1979–2014 are observed. They range from 0.05 Mill. km^2/decade (May) to 0.21 Mill. km^2/decade (June; Table 1). Splitting into two 18-year periods 1979–1996 and 1997–2014 shows accelerating melt rates in all summer months (Table 1). The trend calculations for the seven 30-year moving windows (1979–2008, 1980–2009, etc.) confirm the robustness of the positive trend throughout the period (Figure 2), although most May trends are statistically not significant. Further, this analysis points to a continuous acceleration in June and an increase at the fifth period (1983–2012) in August.

The modeled sea ice melt rate is in general qualitative agreement with the observations with respect to the interannual variability and trend in May–July (Figure 1). But, the simulations also show limitations (Table 1). The model systematically overestimates the melt rates in May–July; the simulated mean rates are by 0.65–0.69 Mill. km^2 higher than in the observations. This seems partly related with the thinner sea ice in the model which can melt faster. The comparison of the simulations with ice thickness data from SHEBA (Surface Heat Budget of the Arctic Ocean; Uttal et al., 2002), ICESat (Ice, Cloud, and Land

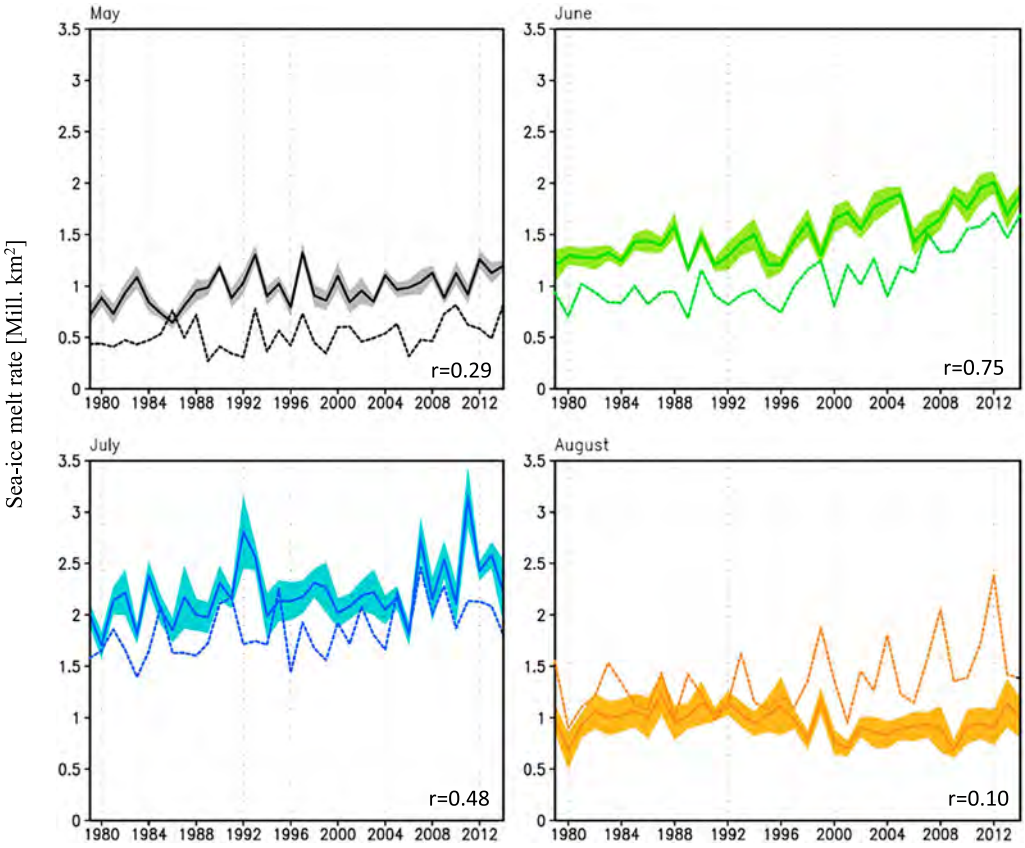

Figure 1. Sea ice melt rate of months May–August from observation (dashed lines) and HIRHAM-NAOSIM simulation (solid lines) for 1979–2014. The solid lines represent the ensemble mean and the shaded areas the 1 standard deviation range of the simulation ensemble. The temporal correlation coefficient (r) between the observed and modeled time series is given in each panel.

Elevation Satellite; Kwok et al., 2009), and the climatology of Bourke and Garrett (1987) showed that the modeled sea ice is partly more than 1 m thinner in the central Arctic compared to observations (Dorn et al., 2009, 2012). On the other hand, the atmospheric conditions contribute to anomalous melting rates (sections 3.2 and 3.3).

The simulated positive melt rate trends in May–July agree with the observations, although the simulated trend is larger than the observed (in May by 60%, in June by 5%, in July by 17%; Table 1). Clearly, the August simulation is an outlier. The amplitude of interannual variability is significantly underestimated and the simulated trend cannot reproduce the observed positive trend. In August, the model reflects the melt rate evolution in the first decades until the end of the 1990s rather well, but cannot simulate the strong increase afterward (Figure 1). This might indicate that the model already melted the thin sea ice in the marginal ice zone such that the reduction of SIE slows down. If one inspects the "compactness" of the sea ice cover (sea ice area divided by sea ice extent), the result shows a decreasing trend, which the model reproduces for all summer months (Figure S2 in the supporting information). This highlights the increasing amount of open water within the ice pack. The observed values are consistently higher than in the model, with largest differences in August. This demonstrates that the unconsolidated sea ice cover (low-concentration sea ice) is overestimated in the model, particularly in August. The melting in the marginal ice zone and the wind-driven closing of open water fractions seem to be too weak in the model.

3.2. Atmospheric Circulation

The summer atmospheric circulation undergoes distinct changes from May to August (Figure 3). At the beginning of the summer (May–June), the dipole SLP pattern is well established, with low pressure over

Table 1
Statistics of Monthly Sea Ice Melt Rate for May–August, Based on 1979–2014 and the First and Second 18-Year Periods (1979–1996 and 1997–2014)

	May	June	July	August
Climatological mean (Mill. km^2)				
1979–2014				
Simulation	1.15	1.74	2.55	1.11
Observation	0.52	1.09	1.86	1.36
1979–1996				
Simulation	1.09	1.53	2.45	1.19
Observation	0.48	0.89	1.76	1.23
1997–2014				
Simulation	1.21	1.95	2.65	1.03
Observation	0.56	1.28	1.95	1.49
Amplitude of interannual variability (Mill. km^2)				
1979–2014				
Simulation	0.78	0.95	1.59	0.63
Observation	0.55	1.02	1.07	1.48
1979–1996				
Simulation	0.78	0.47	1.14	0.58
Observation	0.50	0.47	0.86	0.73
1997–2014				
Simulation	0.48	0.78	1.41	0.48
Observation	0.51	0.90	0.90	1.43
Trend (Mill. km^2/decade)				
1979–2014				
Simulation	0.08*	0.22*	0.14*	−0.05
Observation	0.05*	0.21*	0.12*	0.13*
1979–1996				
Simulation	0.16	0.05	0.22*	0.07
Observation	0.005	−0.02	0.13	−0.03
1997–2014				
Simulation	0.06	0.26*	0.26*	0.05
Observation	0.09	0.39*	0.20*	0.23

Note. The simulation values are based on the 10-member ensemble mean. Trends significant at the 95% level are marked by an asterisk.

Siberia and high pressure over the western Arctic Ocean, particularly over the Beaufort Sea. This SLP pattern involves anticyclonic wind anomalies over the Arctic Ocean, favoring a flow from the Arctic Ocean toward the Fram Strait and enhanced sea ice export into the North Atlantic Ocean (e.g., Matsumura et al., 2014; Ogi et al., 2010; Wernli & Papritz, 2018). With the advance of summer, the pressure gradients become much weaker. In July–August, low pressure occurs over the Arctic Ocean, associated with the maximum in cyclone activity there, and the anticyclonic circulation retreats south into the Beaufort Sea (Figure 3). Accordingly, the Fram Strait outflow becomes weaker (e.g., Serreze & Barry, 2012).

HIRHAM-NAOSIM reproduces these observed patterns of SLP mean and its interannual variability in the summer months (Figure 3). The pattern correlation coefficients between the fields from ERA-Interim and the model simulations are larger than 0.87. Obviously, in August, the model underestimates the SLP interannual variability in the northern Barents/Kara Sea, which is associated with underestimated cyclone frequency and depth (Akperov et al., 2018).

Previous studies showed that mean summer trends are toward increasing SLP over the western Arctic and a strengthening of the Beaufort High, which is related to the warming of the troposphere in the western Arctic and the concomitant reduction in baroclincity (e.g., Ding et al., 2017; Moore, 2012). Wernli and Papritz (2018) found that the trend toward a more anticyclonic summertime circulation in the Arctic manifests in an increased frequency of anticyclones after 2007.

Here we highlight the distinct differences in the observed SLP trend (based on ERA-Interim) from month to month (Figure 4, contours for ERA-Interim). In May, a decreasing SLP over the Arctic Ocean is obvious. In June–August, SLPs show increases over northeastern Canada and over Greenland and the Arctic Ocean. This is indicative of the extension/shift of the Beaufort High and of surface winds becoming more anticyclonic over the Arctic Ocean. Figure 4 shows that the positive SLP trend over the Arctic Ocean is strongest in June and August, but only statistically significant in the latter. These positive trends are accompanied by significant negative SLP trends over the eastern Arctic, especially over Siberia. This dipole pattern of the SLP trends implies enhanced surface winds directed from the Chukchi and East Siberian Seas toward the Fram Strait, which enhances the Transpolar ice drift and contributes to reduced Arctic sea ice (e.g., Inoue & Kikuchi, 2007; Ogi & Wallace, 2007).

We recognize the qualitative and partly even quantitative agreement of the monthly SLP trend patterns in the HIRHAM-NAOSIM simulations with ERA-Interim (Figure 4, color shading for simulations versus contours for ERA-Interim). The pattern correlation coefficients are high and range from 0.85 (August) to 0.95 (June). Still, the model clearly underestimates the trend magnitudes (both the positive and negative) in August. This implies that the model underestimates the strengthening SLP gradient across the Transpolar Sea Ice Drift Stream and from the Barents/Kara Sea toward Northern Greenland, which determines the trend in the surface wind, important for the sea ice export. This model deficit in simulating the significantly strengthened SLP dipole in accordance with the observations is a key contributor to the underestimated acceleration of the sea ice melt rate in the August simulations in recent decades (Figure 1 and section 3.1).

3.3. Relation Between Sea Ice Melt Rate and Atmospheric Conditions

3.3.1. Correlation

As a first benchmark to quantify the relation between sea ice melt rate and atmospheric circulation, we present the correlation between the detrended time series of sea ice melt rate and SLP in summer (May–August) in observations and simulations (Figure 5). A common feature is that summers with high (low) sea ice melt

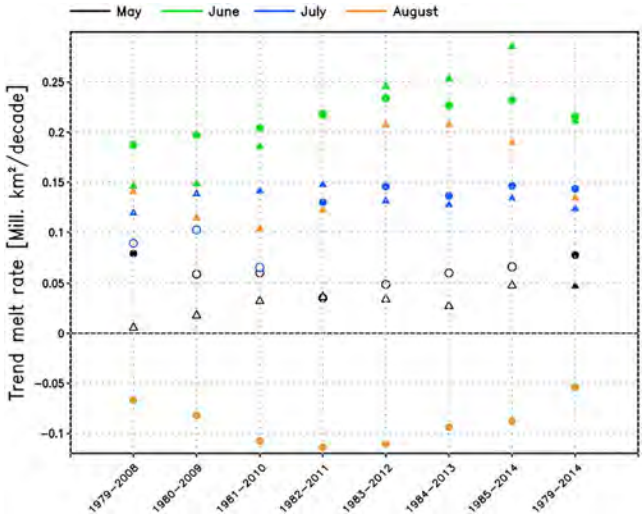

Figure 2. Trends of sea ice melt rate over moving 30-year periods (Mill. km^2/decade) for May–August (color indicates the month) based on observation (triangle) and HIRHAM-NAOSIM simulation (ensemble mean; circle). The first 30-year trend is calculated for the period 1979–2008, the next value shows the trend for 1980–2009, and so on. The last symbol is for the trend of the full 36-year period 1979–2014. Trends significant at the 95% level are indicated by filled triangle or circle; otherwise, the symbol is not filled.

rate are associated with high (low) pressure over the Arctic Ocean and low (high) pressure over Siberia, in accordance with Knudsen et al. (2015). This is equivalent to the previous finding that summers with anomalously low (high) SIE are associated with high (low) SLP anomalies centered over the Arctic Ocean (e.g., Dorn et al., 2012; Ogi & Wallace, 2007; Screen et al., 2011; Serreze et al., 2016). The model reproduces the described observed relationship; the pattern correlation coefficient between the ERA-Interim and HIRHAM-NAOSIM patterns is 0.87.

However, although the correlation is mostly significant, the moderate correlation (coefficients of 0.3–0.5) between sea ice melt rate and SLP indicates that the causal relationship is not straightforward and obviously other SLP patterns and processes play a role as well. For example, inspection of individual September months of highest or lowest SIE shows a wide range of summer atmospheric circulation patterns (Serreze et al., 2016), and the circulation of specific summer months does not reflect the summer average circulation pattern. The correlation patterns between melt rate and SLP differ for the four individual summer months in several aspects, but all agree on the positive correlation over the Arctic Ocean. Furthermore, the strength of the correlation is comparable with that of the summer average (Figure S3 in the supporting information).

3.3.2. SOM Analysis

Both the previous section and analyses by Serreze et al. (2016) illustrate that anomalously high or low sea ice melt rates are associated with more than a single atmospheric circulation pattern. Accordingly, we present here the full variety of summer (May–August) synoptic patterns derived from SOM analysis of ERA-Interim and HIRHAM-NAOSIM

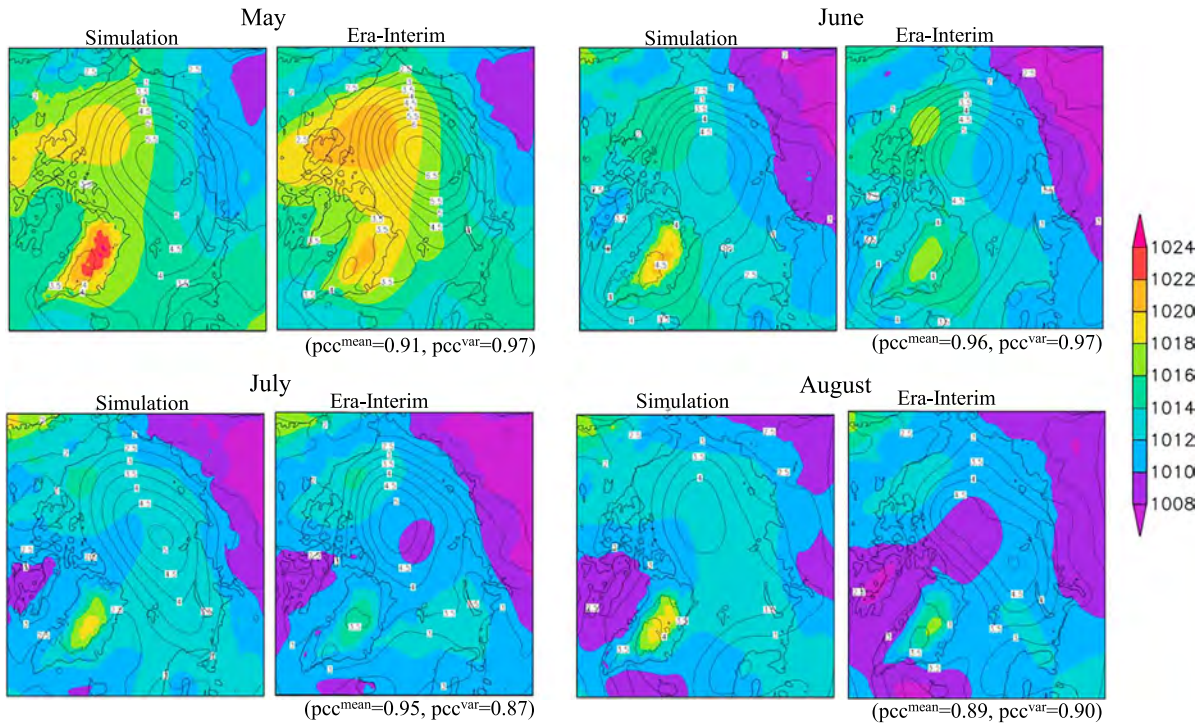

Figure 3. Mean sea level pressure (SLP; hPa) climatological mean (color shading) and interannual variability (isolines) for the months May–August 1979–2014. In the panel for each month, ERA-Interim is shown in the right and HIRHAM-NAOSIM simulation (ensemble mean) is shown in the left. The pattern correlation coefficients between ERA-Interim and modeled mean and variability patterns are given below each monthly panel.

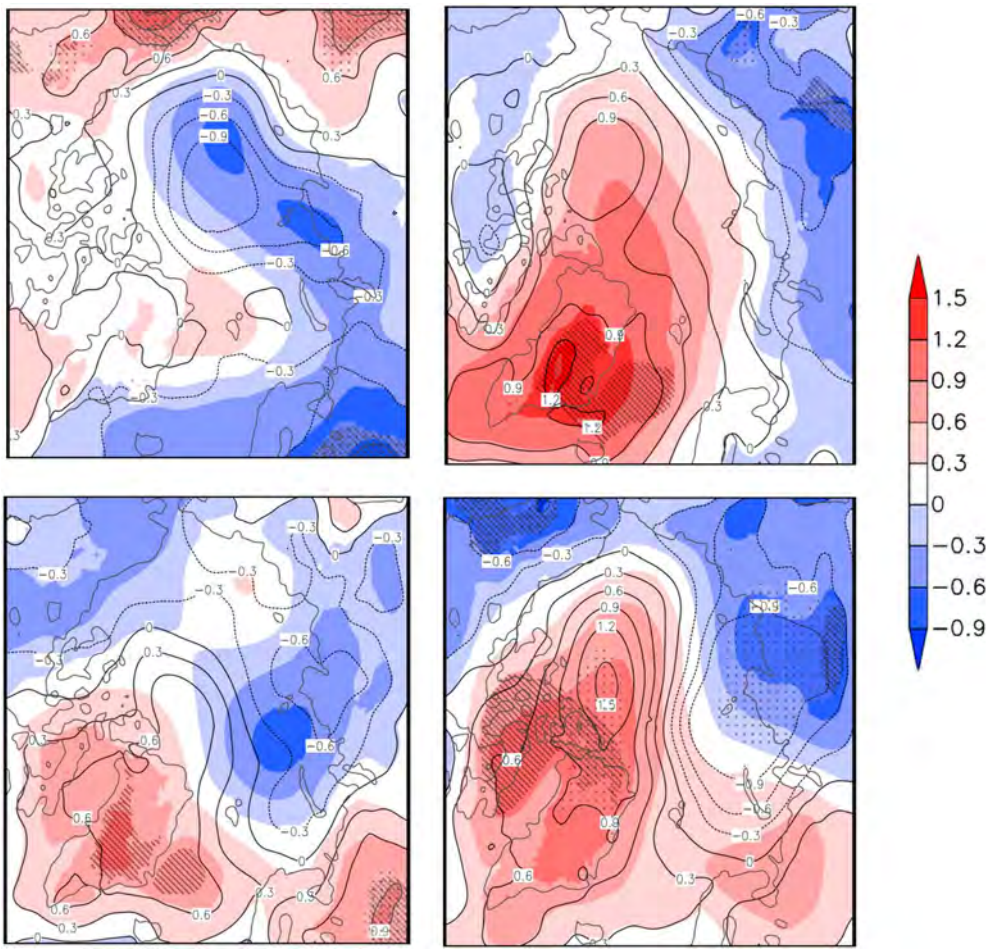

Figure 4. Trend of mean sea level pressure (SLP; hPa/decade) for the months May–August from ERA-Interim (isolines) and HIRHAM-NAOSIM simulation (ensemble mean; color shading) for 1979–2014. Trends significant at the 95% level are indicated by black dots (ERA-Interim) and black hatching (simulation). The pattern correlation coefficient between ERA-Interim and modeled trend patterns is given in the headings.

ensemble simulation data between 1979 and 2014. The so-called "master SOM" provides a complete range of SLP patterns that occur in summer (Figure 6). The two most frequently occurring SLP patterns are labeled (1,0) which represents low pressure over the whole Arctic with a minimum over the central Arctic Ocean and Siberia, and (3,4) which has high pressure over the western part of the Arctic Ocean accompanied with low pressure over Siberia. These are consistent with the "Weak Features" and "Beaufort Highs/Eurasian Lows" most frequent summer patterns identified by Mills and Walsh (2014).

We can classify each of the 20 individual SOM SLP patterns to high and low melt rate (HMR and LMR) conditions in the individual summer months for both ERA-Interim and for each individual ensemble member. The results are summarized in Figure 7, which indicates the relative frequency of occurrence for each SLP pattern in summer under HMR and LMR conditions in the reanalysis and the model ensemble. The absolute numbers of occurrence are also given in Figure S4 in the supporting information. The anomalies are distributed significantly different from expectations based on chance, and Figure 7 clearly indicates that specific SLP patterns are more frequently related with HMR (or LMR) events than other synoptic patterns.

Most HMR conditions can be associated with the occurrence of high pressure over the Arctic Ocean (patterns on the lower right side of the SOM matrix; patterns (2,3), (2,4), (3,4)). This indicates that a strong anticyclone over the central Arctic Ocean favors ice melt. In addition, the strong SLP gradient with the accompanied Siberian low ("dipole pattern") favors ice drift in the Transpolar Drift Stream. This is

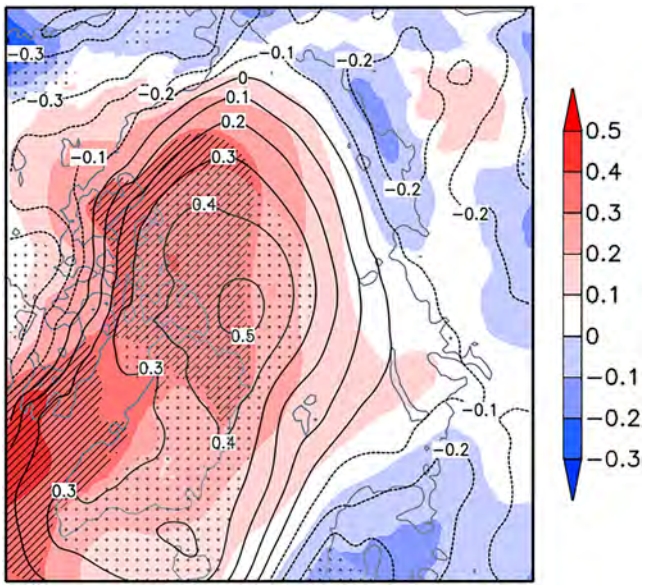

Figure 5. Correlation between sea ice melt rate and mean sea level pressure (SLP), May–August, 1979–2014, based on observation/reanalysis (NSIDC sea ice/ERA-Interim SLP) (isolines) and HIRHAM-NAOSIM simulation (ensemble mean; color shading). Correlations significant at the 95% level are indicated by black dots (observation/reanalysis) and black hatching (simulation).

consistent with our correlation result and other studies (e.g., Mills & Walsh, 2014; Screen et al., 2011), and exemplified by summer 2007 (e.g., Serreze et al., 2016; Wang et al., 2009). In addition, we find that a strong Beaufort High and a cyclone located over northern central Siberia/Taymyr peninsula (patterns (1,2), (3,0), (3,1)) can be associated with HMR conditions. Such patterns are associated with anomalous southerly winds leading to positive temperature anomalies over the Arctic Ocean particularly along the Siberian coast, which favor melting, as was the case for summer 1990 (Serreze et al., 2016).

The patterns in the right part of the SOM matrix occur rarely with LMR conditions. Instead, patterns with cyclonic circulation in the central Arctic are mostly associated with LMR conditions, such as the patterns (0,0), (0,1), and (2,0). Commonly, such negative pressure anomalies over the Arctic Ocean in summer are related with relatively cold conditions, which hamper ice melt, as seen in for example, summer 1996 (Serreze & Stroeve, 2015).

Generally, the model runs agree with the ERA-Interim classification of synoptic patterns to anomalously high and low sea ice melt conditions. This again indicates that the atmospheric circulation-driven mechanisms for anomalous sea ice melt are captured by the model.

However, there are differences in the precise numbers of each pattern between observations and simulations. This might be related with (i) comparing a coupled model which includes the "full" atmosphere-ice interactions with a set of observations/reanalysis which might not be fully consistent (SLP is based on ERA-Interim reanalysis, sea ice is based on satellite data); (ii) that the model represents nonlinearities between sea ice and baroclinic-planetary interactions, including internally

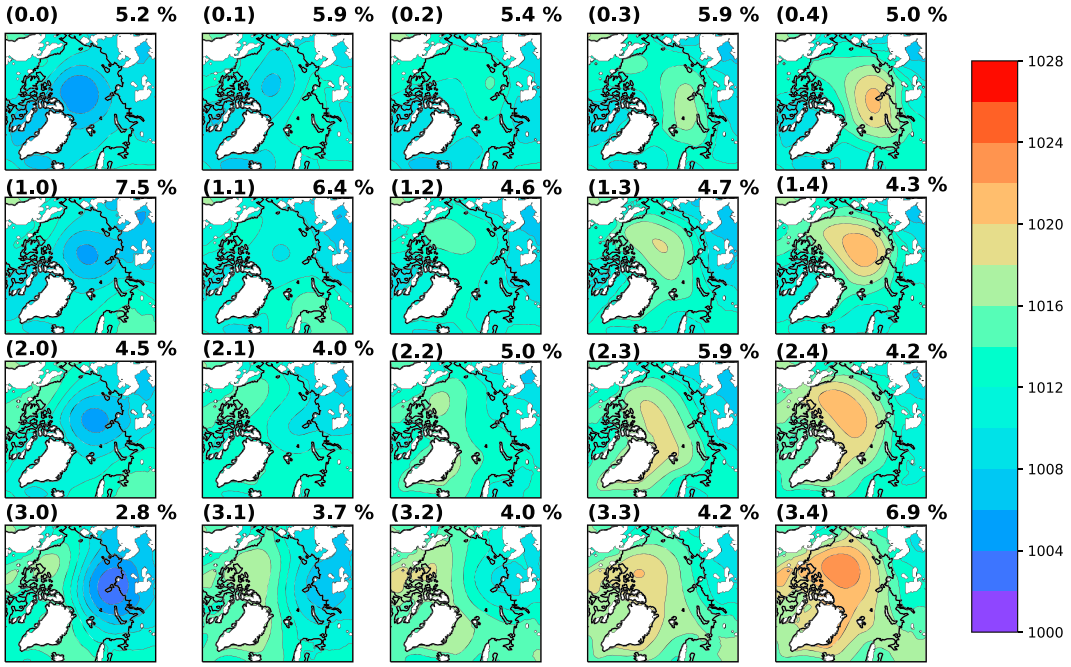

Figure 6. The 5 × 4 master SOM of mean sea level pressure (SLP; hPa) based on summer (May–August) ERA-Interim and HIRHAM-NAOSIM ensemble simulation data from 1979 to 2014. Numbers on the top left of each pattern denote the different patterns and the percentages in the top right of each pattern correspond to the relative frequency of occurrence during the analyzed time period.

Summer SOM pattern relative frequency anomalies

High melt rate

-17	-6	-17	-15	-5	-2	-1	-5	(-17)	2
-2	-9	3	-10	27	3	(8)	4	(-17)	8
(8)	-10	3	-11	-6	4	26	10	8	14
-17	22	3	3	3	-2	-17	7	16	10

Low melt rate

6	6	24	26	-12	1	-12	-8	(-12)	- 3
-4	-2	-12	-1	-1	-14	(-12)	-3	(88)	-8
(38)	17	-12	7	-12	5	3	-11	1	-13
5	-6	-12	5	8	9	5	6	-12	-10

Figure 7. Anomalies of SOM pattern (in %) for summer (May–August) 1979–2016 split by (top) high melt rate (HMR) and (bottom) low melt rate (LMR) conditions based on observations (ERA-Interim SLP/NSIDC sea ice) (left numbers) and HIRHAM-NAOSIM ensemble simulation (right numbers). Anomalies are relative to the expected frequency of pattern occurrence. That is the ratio of the occurrences of each pattern in HMR and LMR months to the total number of times each pattern occurs, which are 17% for observed months classed as HMR and 12% as LMR, while in simulations 18% of months were classed as HMR and 17% as LMR. The anomalies are significantly different from expected by chance at the 95% level for both observations and simulations. Each box of the 5×4 table corresponds with the synoptic patterns at the same position as the master SOM in Figure 6. Agreement in sign of anomaly between observations and simulations are shown in red (positive) and blue (negative). When fewer than five observations are available, the numbers must be interpreted with caution and are bracketed. Absolute numbers are provided in Figure S4 in the supporting information.

generated variability; and (iii) that the master SOM is based on both the reanalysis and ensemble simulations, which gives the simulations more weight. But, we have additionally inspected the SOMs derived separately from the reanalysis and simulations and found them comparable.

3.3.3. Composite Analysis

As another benchmark of circulation-melt rate relationship, we present atmospheric anomalies HMR minus LMR. In the associated Figures 8 and 9, the ERA-Interim results (presented as contours) are shown together with the simulations (color shading).

First, we present the anomalies averaged over the summer (May–August) in Figure 8. The results for SLP support the above-discussed relation that summers with high sea ice melt rate are statistically associated with high pressure over the Arctic Ocean. We calculate statistically significant positive SLP anomalies of up to 5 hPa over the Arctic Ocean under HMR conditions relative to LMR conditions. Overall, the HMR minus LMR SLP pattern resembles the dipole pattern seen in the SLP trend (Figure 4).

ERA-Interim calculates cloud and radiation anomalies associated with the high pressure over the Arctic Ocean under HMR conditions (Figure 8, contours). We detect only small and statistically not significant anomalies in the surface radiation components over the Arctic Ocean in the mean summer response due to cancellation effects of opposite signals in early and late summer. At the beginning of the summer (May), Figure 9 (contours) indicates positive SWD anomalies (up to 15 W/m^2) associated with positive SLP anomalies (up to 7 hPa) and reduced low-level cloud cover and total clouds (not shown) over the Arctic Ocean under HMR conditions. Over the Kara/Barents Sea region with reduced SIE under HMR conditions (Figure S5 in the supporting information), negative SWD anomalies (up to -10 W/m^2) appear due to more open water and increasing cloud cover. With advancing summer and SIE reduction occurring also in the Beaufort, Chukchi, and East Siberian Seas (Figure S5 in the supporting information), negative SWD anomalies (up to -25 W/m^2) and positive LWD anomalies (up to 15 W/m^2) develop over the Arctic Ocean under HMR conditions in late summer (August) due to increasing low-level cloud cover (Figure 9, contours). In summary, positive SWD (LWD) anomalies in early (late) summer can trigger high sea ice melt rates due to cloud-radiation feedback in accordance with Knudsen et al. (2015).

The modeled HMR minus LMR SLP anomaly agrees with ERA-Interim, but the surface radiation anomalies differ considerably (Figures 8 and 9, color shading). While the simulated positive radiation anomaly over the Arctic Ocean in May is in general accordance with ERA-Interim, the model simulates a statistically significant positive SWD anomaly (up to 20 W/m^2) and a small insignificant reduction in LWD over the Arctic Ocean under HMR conditions in August due to reduced low-level clouds (Figure 9, color shading), which is in contradiction to ERA-Interim. Hence, the modeled summer averaged radiation anomalies (positive SWD anomaly of up to 20 W/m^2, slight negative LWD anomaly of up to -3 W/m^2) are entirely contrary to ERA-Interim (Figure 8). The atmospheric anomalies HMR minus LMR based on the ensemble mean (Figure S6 in the supporting information) confirm the reported simulation response.

We do not conclude that the ERA-Interim results for the cloud-radiation feedback reflect the truth, but we demonstrate that cloud feedback in response to sea ice anomalies can be expected. It is known that reanalyses are not in close agreement with satellite and surface observations of cloudiness in the Arctic. In summer, satellite products agree on mean cloudiness of 70–80%, but ERA-Interim shows approximately 10% higher cloudiness. Importantly, such differences can occur due to different spatiotemporal sampling and cloud definition (Zygmuntowska et al., 2012). Further, ERA-Interim shows the highest values of total cloud cover over the central part of the Arctic Ocean, but not over the Norwegian and Barents Seas as observations do (Chernokulsky & Mokhov, 2012; Klaus et al., 2016). Our model results are in agreement with previous

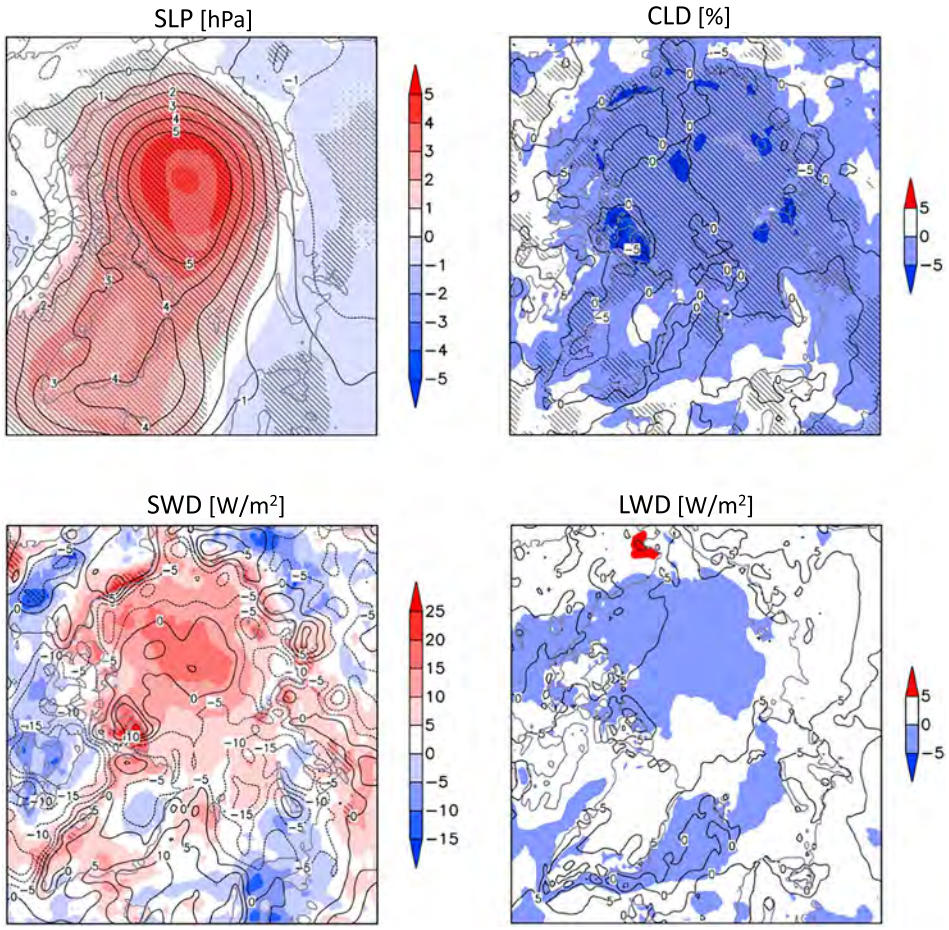

Figure 8. Spatial patterns of atmospheric anomaly "high minus low melt rate" in mean sea level pressure (SLP; hPa), total cloud cover (CLD; %), shortwave downward radiation (SWD; W/m^2), and longwave downward radiation (LWD; W/m^2) at the surface, for May–August 1979–2014, based on ERA-Interim (isolines) and HIRHAM-NAOSIM simulation (color shading). Anomalies significant at the 95% level are indicated by black dots (ERA-Interim) and black hatching (simulation).

studies (Knudsen et al., 2015; Porter et al., 2012; Sato et al., 2012; Schweiger et al., 2008) that reported decreasing low-level cloud cover in response to low-ice conditions and a related decreased static stability and rise in cloud level. Other studies (Eastman & Warren, 2010; Kay & Gettelman, 2009) discussed increased low-level clouds during low-ice years in September, promoted by turbulent heat and moisture transport. Interestingly, Taylor et al. (2015) demonstrated that the cloud properties vary more between different atmospheric regimes (defined by lower static stability) than with the sea ice concentration. And, their regional analysis indicated that the Laptev, Chukchi, and Beaufort Seas show the largest covariance between cloud properties and sea ice in summer and autumn. We still have to conclude that the low-level cloud cover response and the associated cloud-radiation feedback in summer related with anomalous sea ice conditions remains uncertain due to their complexity and limited data. Our finding that this is sensitive to the applied model (or reanalysis) supports the earlier report of Screen et al. (2013). The modeling of Arctic cloud-radiation processes is inherently difficult due to complex interactions between cloud macrophysics and microphysics under the influence of synoptic-scale advection. Among others, the partitioning between cloud liquid water and cloud ice is a critical factor for the cloud radiative effect, but still poorly understood (e.g., Kalesse et al., 2016). Due to the uncertainty in representing Arctic cloud characteristics, such as cloud cover, opacity, phase, and vertical distribution, simulated Arctic clouds and radiation have large biases (e.g., Boeke & Taylor, 2016; English et al., 2015; Lacour et al., 2018; Lenaerts et al., 2017).

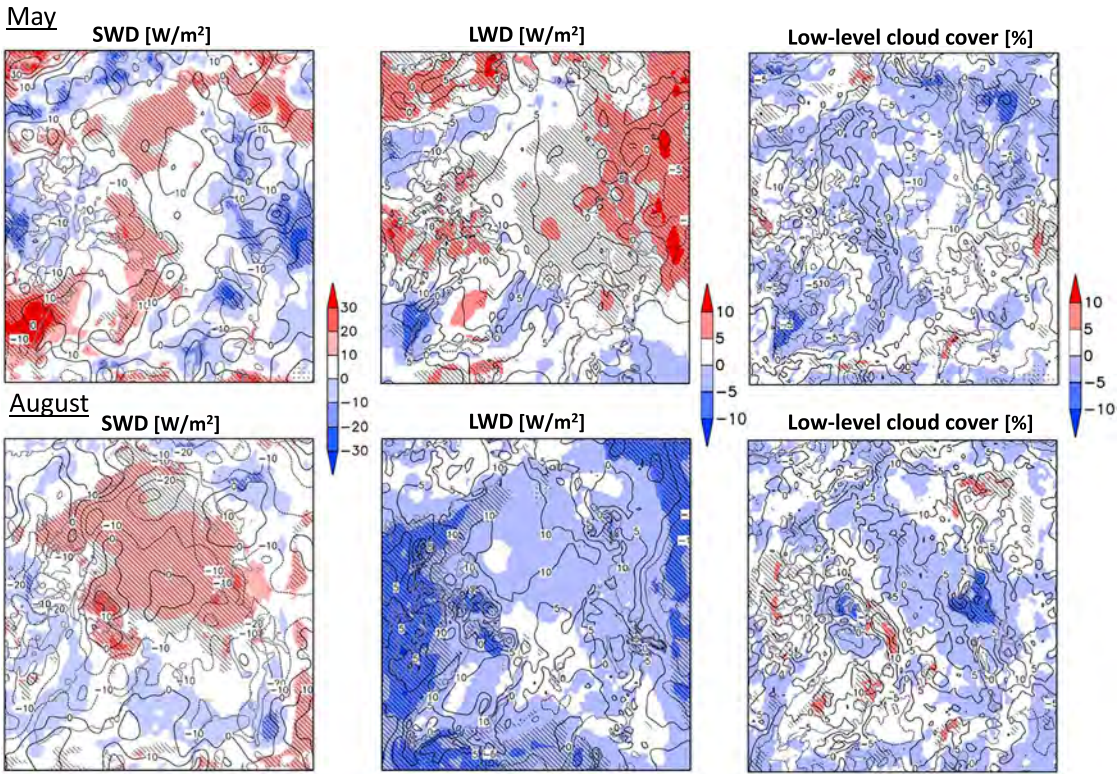

Figure 9. Spatial patterns of atmospheric anomaly "high minus low melt rate" in shortwave downward radiation (SWD; W/m^2) and longwave downward radiation (LWD; W/m^2) at the surface, and low-level cloud cover (%), for (top row) May and (bottom row) August, 1979–2014, based on ERA-Interim (isolines) and HIRHAM-NAOSIM simulation (color shading). Anomalies significant at the 95% level are indicated by black dots (ERA-Interim) and black hatching (simulation).

4. Summary and Conclusions

Observations show a significant positive trend in the summer sea ice melt rate ranging from 0.05 Mill. km^2/decade (May) to 0.21 Mill. km^2/decade (June) for 1979–2014. We recognized a melt rate acceleration in all summer months. This is consistent with atmospheric circulation changes favoring the Arctic Dipole pattern (Overland et al., 2012). This circulation shift is represented by the SLP trend with an increase over the western Arctic and a decrease in Siberia, in accordance with previous studies, which investigated the average summer. In addition, we found that this large-scale dipole SLP trend pattern is strongest in June and August, with little evidence for similar trends in July.

We identified a shortcoming in coupled atmosphere-ocean-sea ice simulations with HIRHAM-NAOSIM in terms of the strengthening SLP dipole in August; that is, the model underestimates the strengthening pressure gradient from the Barents/Kara Sea toward Northern Greenland in recent decades. This is one critical factor for the inadequate simulation of the accelerated sea ice melt rate in August.

Consistent with previous studies, which inspected sea ice extent time series, we showed a statistical relationship between the summer sea ice melt rate and SLP. In addition, we concluded that more than one SLP pattern can be associated with anomalously high melt rate. We showed that specific SLP patterns are clearly more frequently related with a high melt rate than other synoptic patterns. Most HMR cases occur with high pressure over the Arctic Ocean accompanied by low pressure over Siberia ("dipole pattern"), but a strong Beaufort High and an inflow of warm air associated with a cyclone located over the Taymyr peninsula can also trigger anomalous high ice melt. LMR conditions occur in the majority of cases with cyclonic circulation in the central Arctic. Generally, the model arrived at the same classification of SLP patterns related to anomalous melt rates as ERA-Interim.

We further pointed to potential sea ice melt-related cloud-radiation feedback evolving over the summer, but this remains an open issue as ERA-Interim and HIRHAM-NAOSIM showed contrary effects in the low-level clouds. These complex feedback need further study.

Acknowledgments

We gratefully acknowledge the funding by the Deutsche Forschungsgemeinschaft (DFG; German Research Foundation)—project 268020496—TRR 172, within the Transregional Collaborative Research Center "ArctiC Amplification: Climate Relevant Atmospheric and SurfaCe Processes, and Feedback Mechanisms (AC)^3." We thank Paul Hezel and Benjamin Segger for their comments on the manuscript and Ines Hebestadt for the help with the figures. The authors thank two anonymous reviewers for their helpful comments. The ERA-Interim data were obtained from the European Centre for Medium-Range Weather Forecasts (ECMWF; http://apps.ecmwf.int/datasets/data/interim_full_moda/). The sea-ice concentration data were obtained from the National Snow and Sea Ice Data Center (NSIDC; https://nsidc.org/data/NSIDC-0051/). HIRHAM-NAOSIM model data are available at the tape archive of the German Climate Computing Center (DKRZ; https://www.dkrz.de/up/systems/hpss/hpss); one needs to register at DKRZ to get a user account. We will also make the data available via Swift (https://www.dkrz.de/up/systems/swift) on request.

References

Akperov, M., Rinke, A., Mokhov, I. I., Matthes, H., Semenov, V. A., Adakudlu, M., et al. (2018). Cyclone activity in the Arctic from an ensemble of regional climate models (Arctic CORDEX). *Journal of Geophysical Research: Atmospheres*, *123*, 2537–2554. https://doi.org/10.1002/2017JD027703

Boeke, R. C., & Taylor, P. C. (2016). Evaluation of the Arctic surface radiation budget in CMIP5 models. *Journal of Geophysical Research: Atmospheres*, *121*, 8525–8548. https://doi.org/10.1002/2016JD025099

Bourke, R. H., & Garrett, R. P. (1987). Sea ice thickness distribution in the Arctic Ocean. *Cold Regions Science and Technology*, *13*(3), 259–280. https://doi.org/10.1016/0165-232X(87)90007-3

Cavalieri, D. J., Parkinson, C. L., Gloersen, P., & Zwally, H. (1996). *Sea ice concentrations from Nimbus-7 SMMR and DMSP SSM/I-SSMIS Passive Microwave Data*. Boulder, Colorado: National Snow and Ice Data Center. http://nsidc.org/data/docs/daac/nsidc0051_gsfc_seaice.gd.html

Chernokulsky, A., & Mokhov, I. I. (2012). Climatology of total cloudiness in the Arctic: An intercomparison of observations and reanalyses. *Advances in Meteorology*, *2012*, 1–15. https://doi.org/10.1155/2012/542093

Dee, D. P., Uppala, S. M., Simmons, A. J., Berrisford, P., Poli, P., Kobayashi, S., et al. (2011). The ERA-Interim reanalysis: Configuration and performance of the data assimilation system. *Quarterly Journal of the Royal Meteorological Society*, *137*(656), 553–597. https://doi.org/10.1002/qj.828

Ding, Q., Schweiger, A. J., L'Heureux, M. L., Battisti, D. S., Po-Chedley, S., Johnson, N. C., et al. (2017). Influence of high-latitude atmospheric circulation changes on summertime Arctic sea ice. *Nature Climate Change*, *7*(4), 289–295. https://doi.org/10.1038/nclimate3241

Dorn, W., Dethloff, K., & Rinke, A. (2009). Improved simulation of feedbacks between atmosphere and sea ice over the Arctic Ocean in a coupled regional climate model. *Ocean Modelling*, *29*(2), 103–114. https://doi.org/10.1016/j.ocemod.2009.03.010

Dorn, W., Dethloff, K., & Rinke, A. (2012). Limitations of a coupled regional climate model in the reproduction of the observed Arctic sea-ice retreat. *The Cryosphere*, *6*(5), 985–998. https://doi.org/10.5194/tc-6-985-2012

Döscher, R., Vihma, T., & Maksimovich, E. (2014). Recent advances in understanding the Arctic climate system state and change from a sea ice perspective: a review. *Atmospheric Chemistry and Physics*, *14*(24), 13,571–13,600. https://doi.org/10.5194/acp-14-13571-2014

Eastman, R., & Warren, S. G. (2010). Interannual variations of Arctic cloud types in relation to sea ice. *Journal of Climate*, *23*(15), 4216–4232 . https://doi.org/10.1175/2010JCLI3492.1

English, J. M., Gettelman, A., & Henderson, G. R. (2015). Arctic radiative fluxes: Present-day biases and future projections in CMIP5 models. *Journal of Climate*, *28*(15), 6019–6038. https://doi.org/10.1175/JCLI-D-14-00801.1

Graham, R. M., Rinke, A., Cohen, L., Hudson, S. R., Walden, V. P., Granskog, M. A., et al. (2017). A comparison of the two Arctic atmospheric winter states observed during N-ICE2015 and SHEBA. *Journal of Geophysical Research: Atmospheres*, *122*, 5716–5737. https://doi.org/10.1002/2016JD025475

Guemas, V., Blanchard-Wrigglesworth, E., Chevallier, M., Day, J. J., Déqué, M., Doblas-Reyes, F. J., et al. (2016). A review on Arctic sea-ice predictability and prediction on seasonal to decadal time-scales. *Quarterly Journal of the Royal Meteorological Society*, *142*(695), 546–561. https://doi.org/10.1002/qj.2401

Higgins, E. M., & Cassano, J. J. (2009). Impacts of reduced sea ice on winter Arctic atmospheric circulation, precipitation, and temperature. *Journal of Geophysical Research*, *114*, D16107. https://doi.org/10.1029/2009JD011884

Inoue, J., & Kikuchi, T. (2007). Outflow of summertime Arctic sea ice observed by ice drifting buoys and its linkage with ice reduction and atmospheric circulation patterns. *Journal of the Meteorological Society of Japan*, *85*(6), 881–887. https://doi.org/10.2151/jmsj.85.881

Kalesse, H., de Boer, G., Solomon, A., Oue, M., Ahlgrimm, M., Zhang, D., et al. (2016). Understanding rapid changes in phase partitioning between cloud liquid and ice in stratiform mixed-phase clouds: An Arctic case study. *Monthly Weather Review*, *144*, 4805–4826. https://doi.org/10.1175/MWR-D-16-0155.1

Kay, J. E., & Gettelman, A. (2009). Cloud influence on and response to seasonal Arctic sea ice loss. *Journal of Geophysical Research*, *114*, D18204. https://doi.org/10.1029/2009JD011773

Klaus, D., Dethloff, K., Dorn, W., Rinke, A., & Wu, D. L. (2016). New insight of Arctic cloud parameterization from regional climate model simulations, satellite-based and drifting station data. *Geophysical Research Letters*, *43*, 5450–5459. https://doi.org/10.1002/2015GL067530

Knudsen, E. M., Orsolini, Y. J., Furevik, T., & Hodges, K. I. (2015). Observed anomalous atmospheric patterns in summers of unusual Arctic sea ice melt. *Journal of Geophysical Research: Atmospheres*, *120*, 2595–2611. https://doi.org/10.1002/2014JD022608

Kohonen, T. (1998). The self-organizing map. *Neurocomputing*, *21*(1-3), 1–6. https://doi.org/10.1016/S0925-2312(98)00030-7

Kwok, R., Cunningham, G. F., Wensnahan, M., Rigor, I., Zwally, H. J., & Yi, D. (2009). Thinning and volume loss of the Arctic Ocean sea ice cover: 2003–2008. *Journal of Geophysical Research*, *114*, C07005. https://doi.org/10.1029/2009JC005312

Lacour, A., Chepfer, H., Miller, N. B., Shupe, M. D., Noel, V., Fettweis, X., et al. (2018). How well are clouds simulated over Greenland in climate models? Consequences for the surface cloud radiative effect over the ice sheet. *Journal of Climate*, *31*(22), 9293–9312. https://doi.org/10.1175/JCLI-D-18-0023.1

Lenaerts, J. T. M., Van Tricht, K., Lhermitte, S., & L'Ecuyer, T. S. (2017). Polar clouds and radiation in satellite observations, reanalyses, and climate models. *Geophysical Research Letters*, *44*, 3355–3364. https://doi.org/10.1002/2016GL072242

Liu, Y., Weisberg, R. H., & Mooers, C. N. K. (2006). Performance evaluation of the self-organizing map for feature extraction. *Journal of Geophysical Research*, *111*, C05018. https://doi.org/10.1029/2006JA011890

Lynch, A. H., Serreze, M. C., Cassano, E. N., Crawford, A. D., & Stroeve, J. (2016). Linkages between Arctic summer circulation regimes and regional sea ice anomalies. *Journal of Geophysical Research: Atmospheres*, *121*, 7868–7880. https://doi.org/10.1002/2016JDS025164

Matsumura, S., Zhang, X., & Yamazaki, K. (2014). Summer Arctic atmospheric circulation response to spring Eurasian snow cover and its possible linkage to accelerated sea ice decrease. *Journal of Climate*, *27*(17), 6551–6558. https://doi.org/10.1175/JCLI-D-13-00549.1

Meier, W. N., Hovelsrud, G. K., van Oort, B. E. H., Key, J. R., Kovacs, K. M., Michel, C., et al. (2014). Arctic sea ice in transformation: A review of recent observed changes and impacts on biology and human activity. *Review of Geophysics*, *52*, 185–217. https://doi.org/10.1002/2013RG000431

Mills, C. M., & Walsh, J. E. (2014). Synoptic activity associated with sea ice variability in the Arctic. *Journal of Geophysical Research: Atmospheres*, *119*, 12,117–12,131. https://doi.org/10.1002/2014JD021604

Moore, G. W. K. (2012). Decadal variability and a recent amplification of the summer Beaufort Sea High. *Geophysical Research Letters*, *39*, L10807. https://doi.org/10.1029/2012GL051570

Ogi, M., & Wallace, J. M. (2007). Summer minimum Arctic sea ice extent and the associated summer atmospheric circulation. *Geophysical Research Letters*, *34*, L12705. https://doi.org/10.1029/2007GL029897

Ogi, M., Yamazaki, K., & Wallace, J. M. (2010). Influence of winter and summer surface wind anomalies on summer Arctic sea ice extent. *Geophysical Research Letters*, *37*, L07701. https://doi.org/10.1029/2009GL042356

Overland, J. E., Francis, J. A., Hanna, E., & Wang, M. (2012). The recent shift in early summer Arctic atmospheric circulation. *Geophysical Research Letters*, *39*, L19804. https://doi.org/10.1029/2012GL053268

Porter, D. F., Cassano, J. J., & Serreze, M. C. (2012). Local and large-scale atmospheric responses to reduced Arctic sea ice and ocean warming in the WRF model. *Journal of Geophysical Research*, *117*, D11115. https://doi.org/10.1029/2011JD016969

Rinke, A., Dethloff, K., Dorn, W., Handorf, D., & Moore, J. C. (2013). Simulated Arctic atmospheric feedbacks associated with late summer sea ice anomalies. *Journal of Geophysical Research: Atmospheres*, *118*, 7698–7714. https://doi.org/10.1002/jgrd.50584

Rinke, A., Handorf, D., Dorn, W., Dethloff, K., Moore, J. C., & Zhang, X. (2018). Atmospheric feedbacks on Arctic summer sea-ice anomalies in ensemble simulations of a coupled regional climate model. *Advances in Polymer Science*, *29*(3), 156–164. https://doi.org/10.13679/j.advps.2018.3.0015

Sato, K., Inoue, J., Kodama, Y.-M., & Overland, J. E. (2012). Impact of Arctic sea-ice retreat on the recent change in cloud-base height during autumn. *Geophysical Research Letters*, *39*, L10503. https://doi.org/10.1029/2012GL051850

Schweiger, A. J., Lindsay, R. W., Vavrus, S., & Francis, J. A. (2008). Relationships between Arctic sea ice and clouds during autumn. *Journal of Climate*, *21*(18), 4799–4810. https://doi.org/10.1175/2008JCLI2156.1

Screen, J. A., Simmonds, I., Deser, C., & Tomas, R. (2013). The atmospheric response to three decades of observed Arctic sea ice loss. *Journal of Climate*, *26*(4), 1230–1248. https://doi.org/10.1175/JCLI-D-12-00063.1

Screen, J. A., Simmonds, I., & Keay, K. (2011). Dramatic interannual changes of perennial Arctic sea ice linked to abnormal summer storm activity. *Journal of Geophysical Research*, *116*, D15105. https://doi.org/10.1029/2011JD015847

Serreze, M. C., & Barry, R. R. (2011). Processes and impacts of Arctic amplification: A research synthesis. *Global and Planetary Change*, *77*(1-2), 85–96. https://doi.org/10.1016/j.gloplacha.2011.03.004

Serreze, M. C., & Barry, R. R. (2012). *The Arctic climate system*. Cambridge: University press. 402pp

Serreze, M. C., & Stroeve, J. (2015). Arctic sea ice trends, variability and implications for seasonal ice forecasting. *Philosophical transactions Series A, Mathematical, physical, and engineering sciences*, *373*(2045), 20140159. https://doi.org/10.1098/rsta.2014.0159

Serreze, M. C., Stroeve, J., Barrett, A. P., & Boisvert, L. N. (2016). Summer atmospheric circulation anomalies over the Arctic Ocean and their influences on September sea ice extent: A cautionary tale. *Journal of Geophysical Research: Atmospheres*, *121*, 11,463–11,485. https://doi.org/10.1002/2016JD025161

Simmonds, I., & Rudeva, I. (2012). The great Arctic cyclone of August 2012. *Geophysical Research Letters*, *39*, L23709. https://doi.org/10.1029/2012GL054259

Stroeve, J. C., Blanchard-Wrigglesworth, E., Guemas, V., Howell, S., Massonnet, F., & Tietsche, S. (2015). *Developing user-oriented seasonal ice forecasts in a changing Arctic, EOS Trans*, (Vol. 96). Washington, D.C.: AGU. https://doi.org/10.1029/2015EO031431

Stroeve, J. C., Kattsov, V., Barrett, A., Serreze, M., Pavlova, T., Holland, M., & Meier, W. N. (2012). Trends in Arctic sea ice extent from CMIP5, CMIP3 and observations. *Geophysical Research Letters*, *39*, L16502. https://doi.org/10.1029/2012GL052676

Taylor, P. C., Kato, S., Xu, K.-M., & Cai, M. (2015). Covariance between Arctic sea ice and clouds within atmospheric state regimes at the satellite footprint level. *Journal of Geophysical Research: Atmospheres*, *120*, 12,656–12,678. https://doi.org/10.1002/2015JD023520

Uttal, T., Curry, J. A., Mcphee, M. G., Perovich, D. K., Moritz, R. E., Maslanik, J. A., et al. (2002). Surface heat budget of the Arctic ocean. *Bulletin of the American Meteorological Society*, *83*(2), 255–275. https://doi.org/10.1175/1520-0477(2002)083<0255:SHBOTA>2.3.CO;2

Wang, J., Zhang, J., Watanabe, E., Ikeda, M., Mizobata, K., Walsh, J. E., et al. (2009). Is the dipole anomaly a major driver to record lows in Arctic summer sea ice extent? *Geophysical Research Letters*, *36*, 05706. https://doi.org/10.1029/2008GL036706

Wendisch, M., Brückner, M., Burrows, J. P., Crewell, S., Dethloff, K., Ebell, K., et al. (2017). Understanding causes and effects of rapid warming in the Arctic. *EOS, Transactions American Geophysical Union*, *98*. https://doi.org/10.1029/2017EO064803

Wernli, H., & Papritz, L. (2018). Role of polar anticyclones and mid-latitude cyclones for Arctic summertime sea-ice melting. *Nature Geoscience*, *11*(2), 108–113. https://doi.org/10.1038/s41561-017-0041-0

Wittek, P., Gao, S. C., Lim, I. S., & Zhao, L. (2017). somoclu: An efficient distributed library for self-organizing maps. *Journal of Statistical Software*, *78*(9), 1–21. https://doi.org/10.18637/jss.v078.i09

Zhang, J., Lindsay, R., Schweiger, A., & Steele, M. (2013). The impact of an intense summer cyclone on 2012 Arctic sea ice retreat. *Geophysical Research Letters*, *40*, 720–726. https://doi.org/10.1002/grl.50190

Zhang, J., Stegall, S. T., & Zhang, X. (2018). Wind–sea surface temperature–sea ice relationship in the Chukchi–Beaufort Seas during autumn. *Environmental Research Letters*, *13*(3), 034008. https://doi.org/10.1088/1748-9326/aa9adb

Zygmuntowska, M., Mauritsen, T., Quaas, J., & Kaleschke, L. (2012). Arctic clouds and surface radiation—A critical comparison of satellite retrievals and the ERA-Interim reanalysis. *Atmospheric Chemistry and Physics*, *12*(14), 6667–6677. https://doi.org/10.5194/acp-12-6667-2012

Erratum

In the originally published version of this article an incorrect file was included as supporting information. The supporting information has since been corrected, and this version may be considered the authoritative version of record.